ACS APPLIED MATERIALS & INTERFACES

Research Article

www.acsami.org

Co_3O_4/ZnO Nanocomposites: From Plasma Synthesis to Gas Sensing Applications

D. Bekermann,[†] A. Gasparotto,*[,†] D. Barreca,[‡] C. Maccato,[†] E. Comini,[§] C. Sada,[⊥] G. Sberveglieri,[§] A. Devi,[#] and R. A. Fischer[#]

[†]Department of Chemistry, Padova University and INSTM, 35131 Padova, Italy

[‡]CNR-ISTM and INSTM, Department of Chemistry, Padova University, 35131 Padova, Italy

[§]CNR-IDASC, SENSOR Lab, Department of Chemistry and Physics, Brescia University, 25133 Brescia, Italy

[⊥]Department of Physics and CNISM, Padova University, 35131 Padova, Italy

[#]Inorganic Materials Chemistry Group, Lehrstuhl für Anorganische Chemie II, Ruhr-University Bochum, 44780 Bochum, Germany

Supporting Information

ABSTRACT: Herein, we describe the design, fabrication and gas sensing tests of p-Co_3O_4/n-ZnO nanocomposites. Specifically, arrays of ⟨001⟩ oriented ZnO nanoparticles were grown on alumina substrates by plasma enhanced−chemical vapor deposition (PECVD) and used as templates for the subsequent PECVD of Co_3O_4 nanograins. Structural, morphological and compositional analyses evidenced the successful formation of pure and high-area nanocomposites with a tailored overdispersion of Co_3O_4 particles on ZnO and an intimate contact between the two oxides. Preliminary functional tests for the detection of flammable/toxic analytes (CH_3COCH_3, CH_3CH_2OH, NO_2) indicated promising sensing responses and the possibility of discriminating between reducing and oxidizing species as a function of the operating temperature.

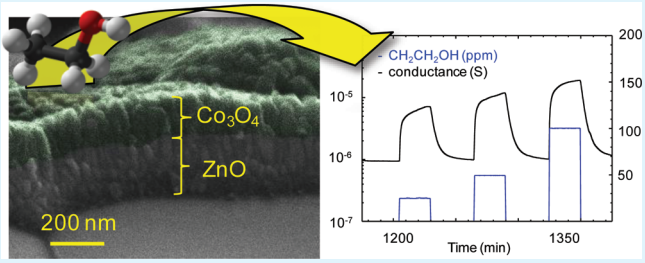

KEYWORDS: *Co_3O_4/ZnO, nanocomposites, plasma enhanced-chemical vapor deposition, gas sensors*

1. INTRODUCTION

Nanocomposites based on the combination of p-type and n-type semiconducting (SC) oxides have come under intense scrutiny for the possibility of joining the intrinsic properties of individual components with the multifunctional behavior exhibited by low-dimensional materials. In this regard, p/n oxide-based nanocomposites have been investigated for various technological applications, such as magnetism, optoelectronics, photocatalysis, and gas sensing.[1−9]

The superior functional performances of these systems in comparison to the corresponding single-phase SC oxides[1,5−7] are mainly ascribed to the build-up of an inner electric field at the p/n junction interface.[3,4,6,9−11] For instance, such a phenomenon is beneficial for optoelectronics, thanks to the resulting rectifying effects, and photocatalysis, because of the enhanced separation of photogenerated electron/hole carriers.[3−6,10,11] As regards gas sensing applications, the combination of p- and n-type nanomaterials can provide higher sensitivities and faster responses due to the formation of a more extended depletion layer.[9,12]

In this context, the present work is focused on p-Co_3O_4/n-ZnO nanocomposites, whose attractive performances have been recently demonstrated for a broad perspective of utilizations.[1,2,9,13,14] The choice of such oxides is motivated by the high technological importance of n-type ZnO, an extremely versatile workhorse for various applications,[2,7,15−19] whereas Co_3O_4, a p-type system, is well-known for its high catalytic activity, in particular in oxidation reactions.[2,9,15,20−22] As a consequence, the synergistic combination of these two SCs paves the way to the development of gas sensors characterized by improved sensitivity/selectivity and mild working temperatures. These issues, along with the long-term stability and limited power dissipitation, are the main challenges to be overcome in order to develop efficient and reliable devices for large-scale utilization.[9,16,20]

The main goal of this study is the fabrication of p-Co_3O_4/n-ZnO composites with tailored properties by a two-step PECVD process, which has never been previously reported for the obtainment of such systems. The initial stage was the deposition of ZnO nanomaterials on Al_2O_3 substrates, followed by the dispersion of Co_3O_4 particles. After a thorough investigation of phase composition and spatial organization as a function of the adopted processing parameters, gas sensing performances were preliminarily investigated in the detection of selected analytes (acetone, ethanol and nitrogen dioxide), interesting for food quality monitoring and environmental purposes.[17,20] It is worth noting that to the best of our knowledge, only one study on the gas sensing properties of

Received: November 15, 2011
Accepted: January 19, 2012
Published: January 19, 2012

Co_3O_4/ZnO nanocomposites is available in the literature up to date.[9]

2. EXPERIMENTAL SECTION

Synthesis. $Zn(ketoimi)_2$ (ketoimi = $[CH_3O(CH_2)_3NC(CH_3)CHC(CH_3)O]$) and $Co(dpm)_2$ (dpm = $(CH_3)_3CC(O)CHC(O)C(CH_3)_3$), selected as zinc and cobalt precursors, were synthesized according to previously reported literature procedures.[23,24] Polycrystalline Al_2O_3 slides (3 × 3 mm^2; thickness = 250 μm) were used as substrates and suitably cleaned prior to each deposition.[16,17] Electronic grade Ar and O_2 were used as plasma sources in a two-electrode custom-built radio frequency (RF) PECVD apparatus (ν = 13.56 MHz). $Zn(ketoimi)_2$ and $Co(dpm)_2$ were vaporized at 150 and 100 °C, respectively, in a reservoir heated by an oil bath, and transported into the reaction chamber by an Ar flow (60 sccm) through heated gas lines to prevent undesired condensation phenomena. Additional O_2 and Ar flows (15 and 20 sccm, respectively) were directly introduced in the reactor. All experiments were performed at a total pressure of 1.0 mbar, using a RF-power of 20 W and an interelectrode distance of 6 cm. For the initial deposition of ZnO, the growth temperature and deposition time were fixed at 300 °C and 60 min, respectively. In the subsequent process step, the amount of Co_3O_4 was tailored as a function of the process duration (10−120 min, growth temperature = 200 °C). Finally, the resulting Co_3O_4/ZnO composites were thermally stabilized by annealing at 400 °C for 60 min in air. In the following, samples will be labeled according to the Co_3O_4 deposition time as: **ZnCo10** (10 min), **ZnCo30** (30 min), **ZnCo60** (60 min), and **ZnCo120** (120 min).

Characterization. Glancing incidence X-ray diffraction (GIXRD) patterns were recorded by means of a Bruker D8 Advance diffractometer equipped with a Göbel mirror and a Cu Kα source (40 kV, 40 mA), at a fixed incidence angle of 3.0°.

Field-emission scanning electron microscopy (FE-SEM) analyses were performed at a primary beam acceleration voltage of 5.0 kV by a Zeiss SUPRA 40VP apparatus. Energy-dispersive X-ray spectroscopy (EDXS) was carried out by an Oxford INCA x-sight X-ray detector using an acceleration voltage of 20 kV.

Secondary ion mass spectrometry (SIMS) measurements were carried out by a IMS 4f mass spectrometer, using a Cs^+ primary beam (14.5 keV, 20 nA, stability = 0.5%). Depth profiles were recorded rastering over a 150 × 150 μm^2 area, collecting negative secondary ions from a subregion close to 7 × 7 μm^2 to avoid crater effects. To improve the in-depth resolution and avoid interference artifacts, we recorded signals in beam blanking mode and using a high mass resolution configuration, performing charge neutralization by means of an electron gun. The deposit thickness was determined as recently described.[20,25]

X-ray photoelectron and X-ray excited Auger electron spectroscopies (XPS and XE-AES) were performed by a VersaProbe spectrometer from Physical Electronics, operating with monochromatic Al Kα (1486.6 eV) radiation, at working pressures lower than 1 × 10^{-9} mbar. Binding energies (BEs, standard deviation = ±0.2 eV) correction for charging was performed by assigning a value of 284.8 eV to the adventitious C1*s* line. Co Auger parameter was calculated as previously reported.[23,26]

Gas Sensing Tests. Gas sensing tests were performed by means of the flow-through technique in a temperature-stabilized sealed chamber (20 °C, atmospheric pressure, relative humidity level = 40%), using a constant synthetic air flow (0.3 L min^{-1}). 200 μm-spaced Pt electrodes and a Pt heater were sputtered on the Co_3O_4 surface and on the backside of the Al_2O_3 substrates, respectively.[16,17,20] A constant bias voltage of 1 V was applied to the specimens and the flowing current was measured through a picoammeter. Measurements were carried out in the range 100−400 °C, after a prestabilization of 8 h at each working temperature. The systems presented a stable and reproducible response. The values of the latter (estimated uncertainty = 5%) were calculated by eqs 1 and 2 for reducing and oxidizing gases, respectively[16]

$$S = (G_f - G_0)/G_0 = \Delta G/G \quad (1)$$

$$S = (R_f - R_0)/R_0 = \Delta R/R \quad (2)$$

where R_0 and G_0 are the initial resistance and conductance values in the presence of synthetic air, and R_f and G_f are the corresponding ones upon contact with the target analyte.

3. RESULTS AND DISCUSSION

Structure, Morphology, and Composition. Basing on our previous results on single-phase Co_3O_4 and ZnO nanosystems,[16,17,20] p-Co_3O_4/n-ZnO nanocomposites were synthesized under optimized conditions, with particular attention on the obtainment of suitably porous ZnO deposits in order to perform the overdispersion of Co_3O_4. The amount of the latter oxide was tailored through proper variation of the deposition time (10−120 min).

Irrespective of the Co_3O_4 content, GIXRD patterns displayed very similar features for the whole samples set (Figure 1).

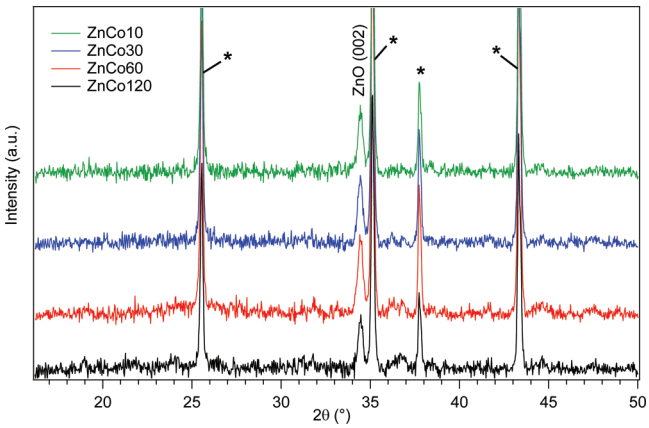

Figure 1. GIXRD patterns of Co_3O_4/ZnO specimens. Stars (*) indicate reflections of the Al_2O_3 substrate.

Beside the reflections of the alumina substrate, the (002) signal of the ZnO zincite phase[27] at 2θ = 34.4° was the only detectable one, indicating the occurrence of a strong ⟨001⟩ preferential orientation of the ZnO component in the nanocomposite materials. Irrespective of the adopted deposition time, peaks pertaining to Co_3O_4 were not clearly evident, suggesting a high dispersion of this oxide over the underlying ZnO layer, and/or low crystallite size. It is also worthwhile observing that the formation of Zn−Co−O ternary phases through solid state reactions between Co_3O_4 and ZnO could be reasonably excluded in the present case, since it usually requires harsh conditions in terms of both temperature and/or applied RF-power.[10,28−31]

The morphology of the synthesized composites was investigated by FE-SEM analyses. In the absence of Co_3O_4, the globular Al_2O_3 substrate particles (0.3−1 μm) were conformally covered by ZnO grains with average lateral and vertical dimensions of 20 and 100 nm, respectively. After Co_3O_4 deposition for 10 min (sample **ZnCo10**), plane-view micrographs (Figure 2a) showed more faceted and slightly bigger particles (~30 nm), and the overall deposit thickness raised to 120 nm, as shown by cross-sectional analyses (Figure 2b). Upon increasing the Co_3O_4 deposition time up to 120 min

dx.doi.org/10.1021/am201591w | ACS Appl. Mater. Interfaces 2012, 4, 928−934

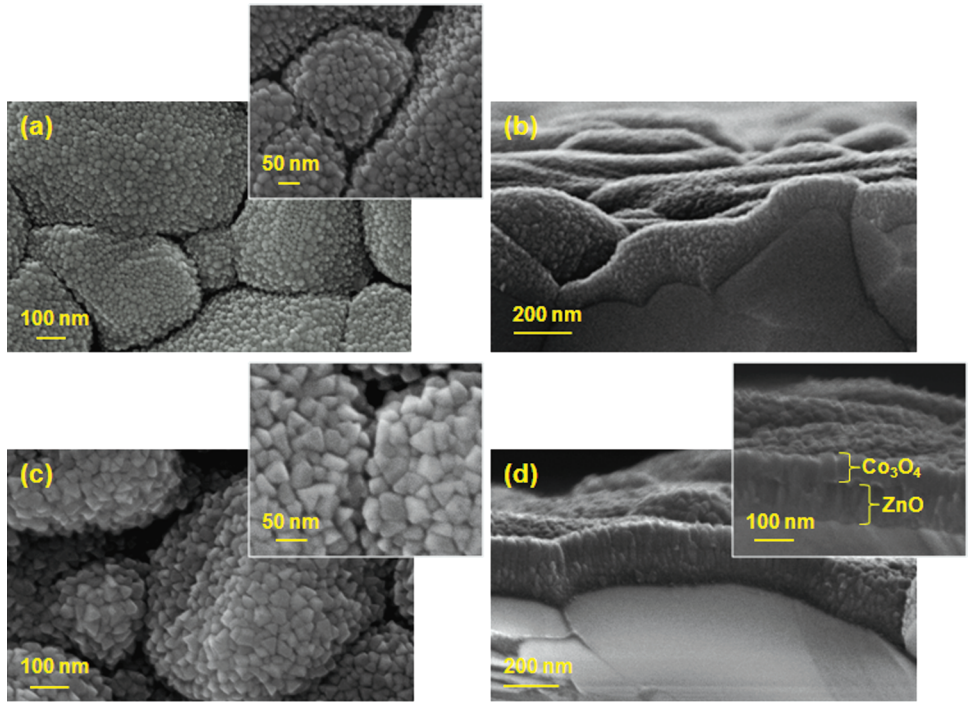

Figure 2. Selected FE-SEM micrographs for: **ZnCo10** (a) plane-view and (b) cross-section; **ZnCo120** (c) plane-view and (d) cross-section. Higher magnification images for a, c, and d are shown as insets.

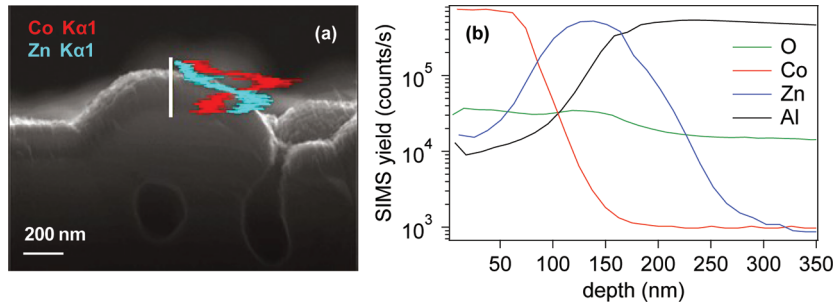

Figure 3. (a) Cross-sectional EDXS line-scan and (b) SIMS depth profile for sample **ZnCo120**.

(sample **ZnCo120**, Figure 2c, d), the observed nanograins had an average size of ∼40 nm and exhibited well-evident pyramidal-like morphology, as often reported for face-centered cubic systems like Co_3O_4.[26,32] The mean deposit thickness was found to be 180 nm. The corresponding cross-sectional analyses (Figure 2d) suggested the existence of two separated phases, attributed to a Co_3O_4 deposit (∼80 nm thick) on a ZnO matrix of approximately 100 nm. The high roughness and reduced particle size characterizing the present Co_3O_4/ZnO composites suggest a high active area, anticipating attractive gas sensing performances. In addition, the overdispersion of Co_3O_4 on ZnO results in an intimate contact between the two oxides, enabling a favorable exploitation of their mutual electronic interactions.[25]

Further information on the Co_3O_4 and ZnO vertical distribution was obtained by in-depth compositional analyses. The Co and Zn weight percentages averaged over the entire deposit thickness were obtained by EDXS, yielding a Co:Zn ratio increasing from 4:96 (**ZnCo10**) to 37:63 (**ZnCo120**; see also Figure S1 and related comments). Figure 3a displays a cross-section EDXS line-scan of sample **ZnCo120**, showing a net predominance of cobalt over zinc in the outermost sample region. Conversely, the Zn Kα1 intensity underwent a progressive increase in the inner system region at expenses of the Co Kα1 one, confirming thus the predominance of ZnO in proximity of the Al_2O_3 substrate, as already discussed in relation to Figure 2d.

A deeper insight into the system composition was obtained by SIMS, and a representative in-depth profile is shown in Figure 3b. In general, the negligible C content (<35 ppm) evidenced the high purity of the obtained materials. In line with the above-discussed results, Co_3O_4 was predominant in the outermost deposit region, and the corresponding estimated thickness from the analysis of the Co SIMS profile was ∼80 nm, as also derived from FE-SEM. Below this layer, the Zn ionic yield underwent a progressive increase and a subsequent intensity reduction in the proximity of the Al_2O_3 substrate, i.e., upon increasing the Al signal. These data, in line with EDXS results, pointed out to the obtainment of bilayered composites, with zinc oxide being confined in the inner system region. The corresponding ZnO thickness was estimated to be 100 nm, in good agreement with FE-SEM results (see above).

To investigate the possible surface copresence of both the single oxides[1,28] and the exposure of different surface sites in

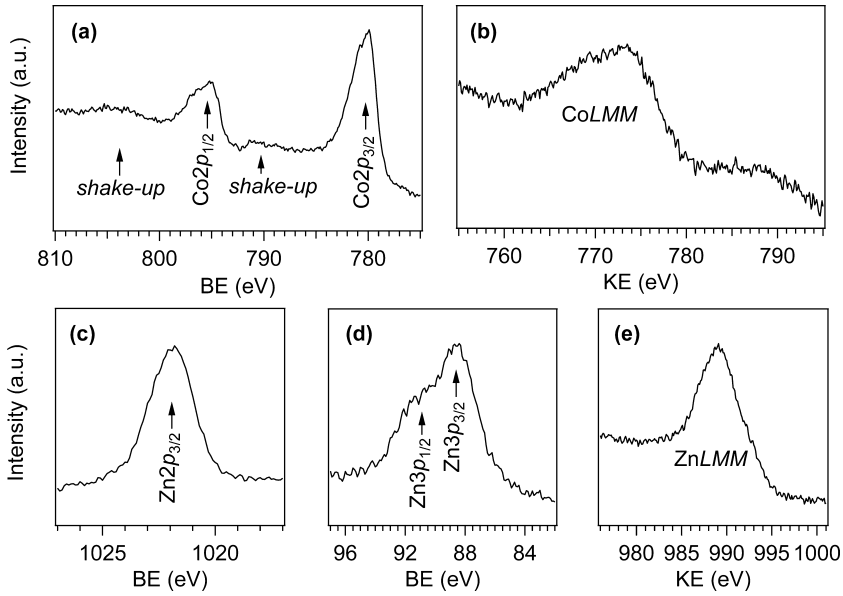

Figure 4. Representative XPS and XE-AES surface peaks for (a, b) cobalt and (c–e) zinc in Co_3O_4/ZnO nanocomposites (specimen **ZnCo10**).

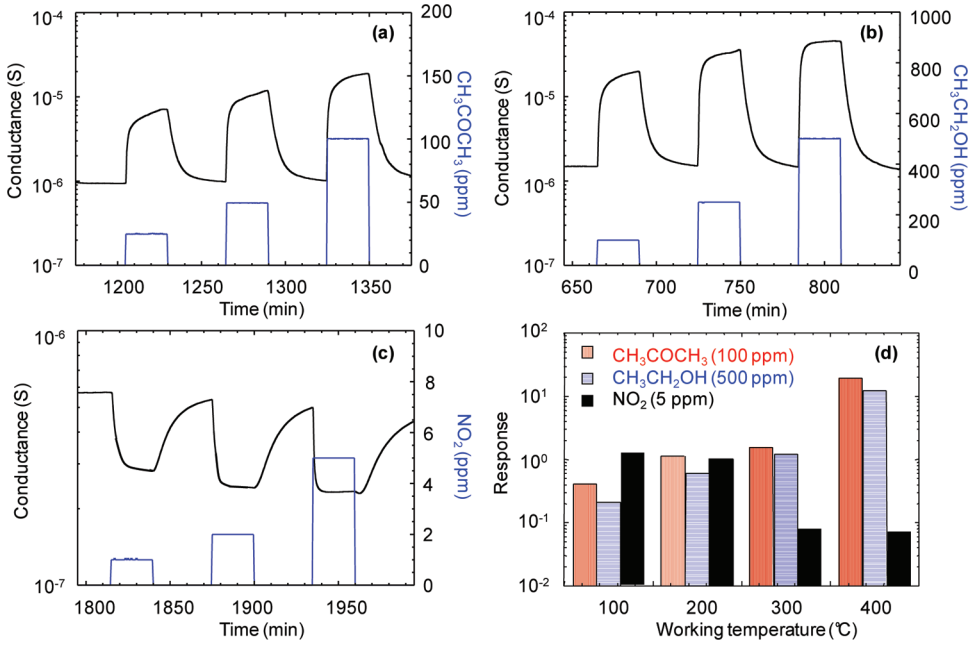

Figure 5. Gas sensing responses (black) of a Co_3O_4/ZnO sensor (specimen **ZnCo10**) toward square concentration pulses (blue) of (a) CH_3COCH_3, (b) CH_3CH_2OH, and (c) NO_2. Working temperatures = (a, b) 400 and (c) 200 °C. (d) Dependence of the response on the operating temperature for selected analyte concentrations (specimen **ZnCo10**).

view of sensing experiments, we undertook XPS and XE-AES analyses. For all samples, surface spectra evidenced the presence of C and O signals, the former being limited to the system surface (see also SIMS data), as already reported for pure Co_3O_4 and ZnO systems.[3,16,20,33,34] The main contribution to the C1*s* peak at BE = 284.8 eV was due to adventitious carbon, whereas a weak shoulder centered at BE = 288.2 eV was related to chemisorbed surface carbonates.[3,20,33,34] Two bands contributed to the O1*s* signal, a main one at BE = 529.9 eV ascribed to lattice oxygen, and a minor component at 531.6 eV, assigned to carbonates and hydroxyl groups.[16] Interestingly, the surface presence of zinc demonstrated the dispersion of Co_3O_4 particles in the ZnO matrix, without complete coverage of the latter. In fact, irrespective of the Co_3O_4 deposition time, Zn and Co signals were always detected on the sample surface. The measured Co:Zn atomic ratio increased with Co_3O_4 deposition time, i.e. from 1.7 (**ZnCo10**) to 2.0 (**ZnCo120**). This result indicates that, despite the conformal coverage of ZnO by Co_3O_4, a residual porosity is still present at the interface between the two phases. Such a feature, together with the formation of nanosized p-Co_3O_4/n-ZnO heterojunctions, is extremely promising for gas sensing applications.[12]

The most representative Co and Zn XPS and XE-AES signals are displayed in Figure 4. In line with previous works, the positions of Co2$p_{3/2}$ (BE = 780.3 eV, Figure 4a) and Co*LMM* peaks [kinetic energy (KE) = 771.9 eV, Figure 4b] were in agreement with the formation of Co_3O_4, excluding thus the presence of CoO and/or Co–Zn–O ternary phases.[1,20,33] This

dx.doi.org/10.1021/am201591w | *ACS Appl. Mater. Interfaces* 2012, 4, 928–934

assignment was also supported by the low intensity of shake-up satellites and by the calculation of the Auger α parameter, yielding a value of 1552.2 eV.[1,33] Concerning zinc, the presence of ZnO was confirmed by the position of Zn2$p_{3/2}$ (BE = 1021.8 eV), Zn3p (BE = 88.3 eV), and Zn*LMM* (KE = 989.1 eV) photopeaks (Figures 4c–e).[1,3] The absence of any BE shift for the Co and Zn signals as a function of the Zn/Co ratio further supported the presence of the two separate phases.[1]

Gas Sensing Tests. Preliminary investigation of the composite functional performances were addressed at the detection of acetone, ethanol and nitrogen dioxide, and selected dynamic responses are displayed in Figure 5a–c. As can be observed, the measured conductance underwent an increase in the presence of reducing gases (CH_3COCH_3, CH_3CH_2OH, Figure 5a, b), whereas the opposite phenomenon was revealed upon contact with NO_2, an oxidizing analyte (Figure 5c). Such a behavior, typical for n-type SCs,[8,17] was related to the higher overall content of the ZnO phase with respect to Co_3O_4 (see above). Furthermore, for all the tested analytes the conductance variation progressively increased with the gas concentration, enabling to rule out any appreciable saturation effect under the adopted conditions. Finally, the almost complete recovery of the baseline conductance values at the end of each pulse indicated a reversible interaction between the sensing element and the target analytes, a key issue in view of eventual technological applications.

The generally accepted sensing mechanism for similar SC systems is based on the initial dissociative chemisorption of oxygen at the sensor surface, resulting in the formation of negatively charged oxygen species.[8,9,16,17,20,35] Upon adsorption of CH_3CH_2OH or CH_3COCH_3, oxygen species promote their oxidation to CO_2 and H_2O and the concomitant release of electrons into the ZnO conduction band, increasing thus the concentration of main charge carriers and, hence, the measured conductance. In a different way, upon sensing of an oxidizing gas, such as NO_2, electrons are withdrawn from the SC surface, resulting in a conductance decrease. Irrespective of the target gas, the sharp conductance variation observed upon analyte injection, followed by a slower increase up to the end of the pulse, suggested that the analyte chemisorption was the rate-determining step for the overall process.[16,25]

In view of practical applications, the sensor selectivity is a key concern and, at the same time, an open problem still far from being completely solved.[9,25] In the present work, the selectivity toward reducing or oxidizing gases could be controlled as a function of the sensor working temperature (Figure 5d). Indeed, at 100 °C, the measured responses to NO_2 (>1) were higher than the corresponding values for CH_3COCH_3 and CH_3CH_2OH. Conversely, for working temperatures higher than 200 °C, the response to nitrogen dioxide progressively lowered, and a net increase of the responses to reducing gases was detected at 400 °C, yielding values higher than 10. These results are of interest in view of technological exploitation of the current sensors in the presence of gas mixtures, as usually occurring under real-world conditions.

The response of nanocomposites characterized by different Co_3O_4 deposition times toward fixed concentrations of CH_3COCH_3, CH_3CH_2OH, and NO_2 are displayed in Figure 6. As can be observed, irrespective of the target analyte, the system performances decreased on going from sample **ZnCo10** to **ZnCo120**. This result can be likely ascribed to the concurrence of two main factors, i.e. the increased Co_3O_4 particle size and the partial reduction of the system porosity for

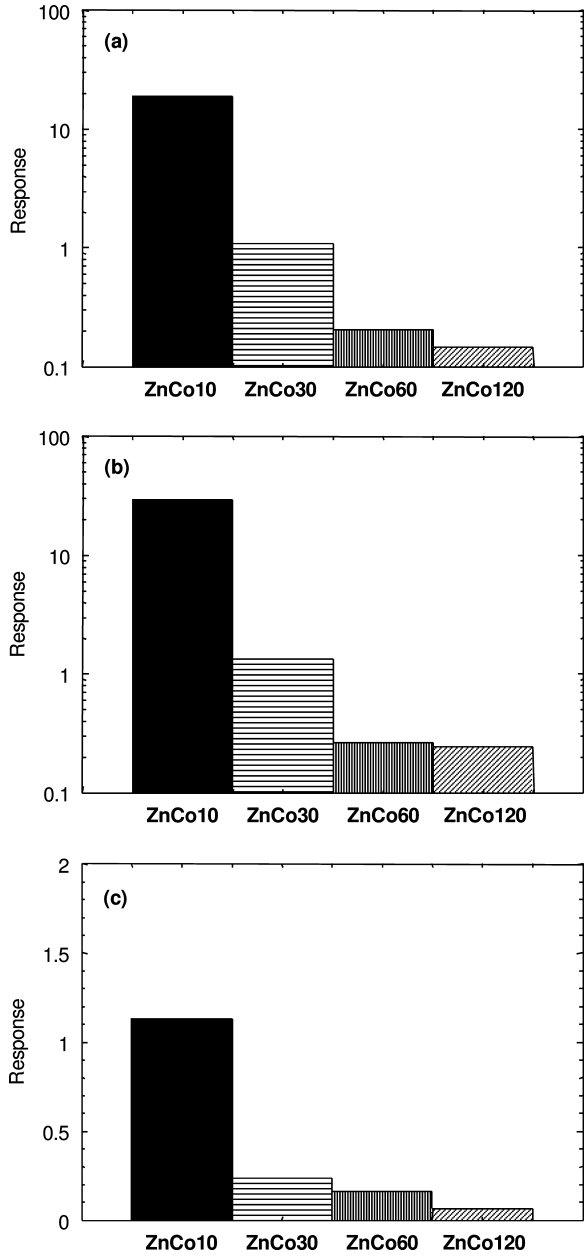

Figure 6. Response toward (a) 100 ppm CH_3COCH_3, (b) 500 ppm CH_3CH_2OH, and (c) 5 ppm NO_2 for nanocomposites characterized by a different Co_3O_4 deposition time. Working temperatures = (a, b) 400 and (c) 200 °C.

the highest cobalt oxide loadings (see also comments to Figure 7). These findings indicate that the best performances correspond to a Co/Zn ratio ensuring, at the same time, an efficient interfacial contact between ZnO and Co_3O_4 and a high surface area available for gas adsorption.

In the case of specimen **ZnCo10**, where such conditions are likely fulfilled, the sensor performances result appreciably better than those of our previous studies on pure, Au-doped or F-doped Co_3O_4,[20,26] and comparable to the results obtained by Na et al.,[9] the only work on Co_3O_4/ZnO gas sensors reported so far. Such results can be explained by considering that p-Co_3O_4/n-ZnO junctions produce an improved charge separation at the interface between the two oxides, generating, in turn, an enhanced conductance modulation upon interaction with the target gases (Figure 7).

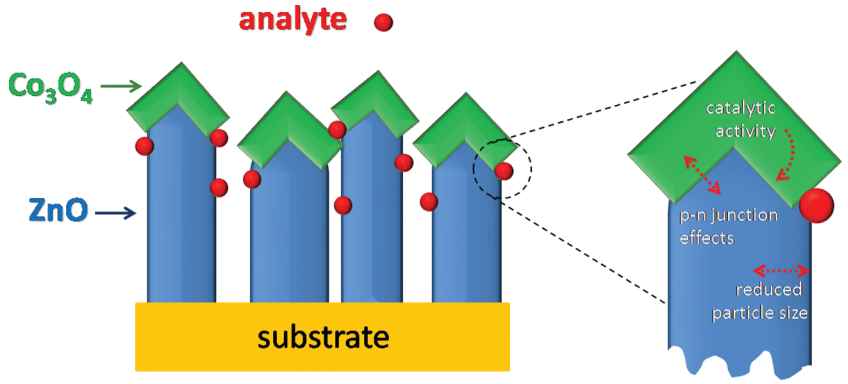

Figure 7. Schematic representation of the main phenomena beneficially affecting the gas sensing behavior of the present Co_3O_4/ZnO nanocomposites.

In this context, the reduced particle size and the well-known catalytic activity of cobalt oxide are believed to play a further beneficial role on the functional behavior.[9] It is worth observing that whereas n-type metal oxides only chemisorb as much oxygen as necessary to compensate their deficiencies, the concentration of surface oxygen on p-type SCs is significantly higher.[20,35] As a consequence, the copresence of Co_3O_4 and ZnO, with an intimate contact between them, can further contribute to the improvement of the composite sensor performances.

To validate the above observations, a bare Co_3O_4 film was grown directly on Al_2O_3 adopting the same synthesis conditions used for cobalt oxide in specimen **ZnCo10**. As expected, upon exposure to reducing gases such as acetone or ethanol (see Figure S2 in the Supporting Information), Co_3O_4 displayed a conductance reduction, in line with its p-type behavior.[20] Apart from this difference with respect to sample **ZnCo10**, the response values extrapolated by Figure S2 were more than 1 order of magnitude lower than the ones obtained for the corresponding Co_3O_4/ZnO composite under the same testing conditions (see also Figures 5 and 6). As previously discussed, these findings highlight beneficial synergistic effects originating from Co_3O_4/ZnO coupling. Similar results were also observed for the detection of NO_2.

In the literature, ZnO deposits with thickness comparable to the zinc oxide layer of the present Co_3O_4/ZnO nanocomposites have been reported to display gas sensing performances both higher or lower that the ones reported above.[17,36−39] Such issue indicates that, beside film thickness, gas sensing performances are also affected by other parameters (e.g., crystallite size, surface area, defect content,...), evidencing thus the importance of both material design and morphological/structural control.

4. CONCLUSIONS

In this work, p-Co_3O_4/n-ZnO composites were synthesized by a two-step PECVD process, consisting in the initial ZnO growth on Al_2O_3 substrates and the overdispersion of Co_3O_4 particles, whose amount was tailored as a function of deposition time. An extensive characterization of the system structure, morphology and composition by GIXRD, FE-SEM, EDXS, SIMS, XPS and XE-AES showed a conformal coverage of ⟨001⟩ oriented ZnO nanocolumns by low-sized Co_3O_4 grains, leading to an intimate contact between the two single-phase oxides. Preliminary tests in the detection of reducing (CH_3CH_2OH, CH_3COCH_3) and oxidizing (NO_2) gases evidenced attractive functional performances in terms of both responses and selectivity. Such results can be attributed to the copresence of several beneficial phenomena: (i) the reduced particle size, enabling enhanced conductance modulations upon interaction with the target analytes; (ii) p/n junction effects at the Co_3O_4/ZnO interface, inducing an extension of the electron depletion layer; (iii) the Co_3O_4 catalytic activity, promoting the chemical reactions taking place during the sensing process.

Overall, the presented studies are of high significance for the development of selective sensor devices with improved functional properties. In addition, the adopted synthesis strategy opens intriguing perspectives for the design of p/n composite nanoarchitectures for different kinds of applications, from heterogeneous catalysis to photoinduced pollutant degradation and ferromagnets in spintronic devices. Efforts in this direction are currently underway.

■ ASSOCIATED CONTENT

Ⓢ Supporting Information

Additional figures and information (PDF). This material is available free of charge via the Internet at http://pubs.acs.org.

■ AUTHOR INFORMATION

Corresponding Author

*E-mail: alberto.gasparotto@unipd.it.

Notes

The authors declare no competing financial interest.

■ ACKNOWLEDGMENTS

The research leading to these results has received funding from the European Community's Seventh Framework Program (FP7/2007-2013) under grant agreement ENHANCE-238409, as well as from Padova University PRAT 2010 (CPDA102579) project. K. Xu and M. Banerjee (Ruhr-University Bochum, Germany) are gratefully acknowledged for technical assistance in the Zn precursor synthesis and XPS analysis.

■ REFERENCES

(1) Martín-González, M. S.; Fernández, J. F.; Rubio-Marcos, F.; Lorite, I.; Costa-Kramer, J. L.; Quesada, A.; Bañares, M. A.; Fierro, J. L. G. *J. Appl. Phys.* **2008**, *103*, 083905.

(2) Kanjwal, M. A.; Sheikh, F. A.; Barakat, N. A. M.; Chronakis, I. S.; Kim, H. Y. *Appl. Surf. Sci.* **2011**, *257*, 7975−7981.

(3) Zhang, Z. Y.; Shao, C. L.; Li, X. H.; Wang, C. H.; Zhang, M. Y.; Liu, Y. C. *ACS Appl. Mater. Interfaces* **2010**, *2*, 2915−2923.

(4) Hsieh, J. H.; Kuo, P. W.; Peng, K. C.; Liu, S. J.; Hsueh, J. D.; Chang, S. C. *Thin Solid Films* **2008**, *516*, 5449−5453.
(5) Shifu, C.; Wei, Z.; Wei, L.; Huaye, Z.; Xiaoling, Y. *Chem. Eng. J.* **2009**, *155*, 466−473.
(6) Kim, H. G.; Borse, P. H.; Choi, W. Y.; Lee, J. S. *Angew. Chem., Int. Ed.* **2005**, *44*, 4585−4589.
(7) Hong, R. Y.; Zhang, S. Z.; Di, G. Q.; Li, H. Z.; Zheng, Y.; Ding, J.; Wei, D. G. *Mater. Res. Bull.* **2008**, *43*, 2457−2468.
(8) Hwang, I. S.; Choi, J. K.; Kim, S. J.; Dong, K. Y.; Kwon, J. H.; Ju, B. K.; Lee, J. H. *Sens. Actuators, B* **2009**, *142*, 105−110.
(9) Na, C. W.; Woo, H.-S.; Kim, I.-D.; Lee, J.-H. *Chem. Commun.* **2011**, *47*, 5148−5150.
(10) Zhuge, L. J.; Wu, X. M.; Wu, Z. F.; Yang, X. M.; Chen, X. M.; Chen, Q. *Mater. Chem. Phys.* **2010**, *120*, 480−483.
(11) Vanaja, K.; Bhatta, U.; Ajimsha, R.; Jayalekshmi, S.; Jayaraj, M. *Bull. Mater. Sci.* **2008**, *31*, 753−758.
(12) Chowdhuri, A.; Sharma, P.; Gupta, V.; Sreenivas, K.; Rao, K. V. *J. Appl. Phys.* **2002**, *92*, 2172−2180.
(13) Uriz, I.; Arzamendi, G.; López, E.; Llorca, J.; Gandía, L. M. *Chem. Eng. J.* **2011**, *167*, 603−609.
(14) Rubio-Marcos, F.; Calvino-Casilda, V.; Bañares, M. A.; Fernandez, J. F. *J. Catal.* **2010**, *275*, 288−293.
(15) Tak, Y.; Yong, K. *J. Phys. Chem. C* **2008**, *112*, 74−79.
(16) Barreca, D.; Bekermann, D.; Comini, E.; Devi, A.; Fischer, R. A.; Gasparotto, A.; Maccato, C.; Sberveglieri, G.; Tondello, E. *Sens. Actuators, B* **2010**, *149*, 1−7.
(17) Barreca, D.; Bekermann, D.; Comini, E.; Devi, A.; Fischer, R. A.; Gasparotto, A.; Maccato, C.; Sada, C.; Sberveglieri, G.; Tondello, E. *CrystEngComm* **2010**, *12*, 3419−3421.
(18) Huang, M. H.; Mao, S.; Feick, H.; Yan, H. Q.; Wu, Y. Y.; Kind, H.; Weber, E.; Russo, R.; Yang, P. D. *Science* **2001**, *292*, 1897−1899.
(19) Wang, Z. Q.; Gong, J. F.; Su, Y.; Jiang, Y. W.; Yang, S. G. *Cryst. Growth Des.* **2010**, *10*, 2455−2459.
(20) Barreca, D.; Bekermann, D.; Comini, E.; Devi, A.; Fischer, R. A.; Gasparotto, A.; Gavagnin, M.; Maccato, C.; Sada, C.; Sberveglieri, G.; Tondello, E. *Sens. Actuators, B* **2011**, *160*, 79−86.
(21) Ma, C. Y.; Mu, Z.; Li, J. J.; Jin, Y. G.; Cheng, J.; Lu, G. Q.; Hao, Z. P.; Qiao, S. Z. *J. Am. Chem. Soc.* **2010**, *132*, 2608−2613.
(22) Yu, Y. B.; Takei, T.; Ohashi, H.; He, H.; Zhang, X. L.; Haruta, M. *J. Catal.* **2009**, *267*, 121−128.
(23) Barreca, D.; Massignan, C.; Daolio, S.; Fabrizio, M.; Piccirillo, C.; Armelao, L.; Tondello, E. *Chem. Mater.* **2001**, *13*, 588−593.
(24) Bekermann, D.; Rogalla, D.; Becker, H. W.; Winter, M.; Fischer, R. A.; Devi, A. *Eur. J. Inorg. Chem.* **2010**, *2010*, 1366−1372.
(25) Barreca, D.; Carraro, G.; Comini, E.; Gasparotto, A.; Maccato, C.; Sada, C.; Sberveglieri, G.; Tondello, E. *J. Phys. Chem. C* **2011**, *115*, 10510−10517.
(26) Barreca, D.; Comini, E.; Gasparotto, A.; Maccato, C.; Pozza, A.; Sada, C.; Sberveglieri, G.; Tondello, E. *J. Nanosci. Nanotechnol.* **2010**, *10*, 8054−8061.
(27) JCPDS, pattern no. 36−1451, 2000.
(28) Wei, L.; Li, Z. H.; Zhang, W. F. *Appl. Surf. Sci.* **2009**, *255*, 4992−4995.
(29) Yang, S. G.; Pakhomov, A. B.; Hung, S. T.; Wong, C. Y. *IEEE Trans. Magn.* **2002**, *38*, 2877−2879.
(30) Sudakar, C.; Kharel, P.; Lawes, G.; Suryanarayanan, R.; Naik, R. *Appl. Phys. Lett.* **2008**, *92*, 062501.
(31) Bhargava, R.; Sharma, P. K.; Dutta, R. K.; Kumar, S.; Pandey, A. V.; Kumar, N. *Mater. Chem. Phys.* **2010**, *120*, 393−398.
(32) Barreca, D.; Gasparotto, A.; Lebedev, O. I.; Maccato, C.; Pozza, A.; Tondello, E.; Turner, S.; Van Tendeloo, G. *CrystEngComm* **2010**, *12*, 2185−2197.
(33) Barreca, D.; Devi, A.; Fischer, R. A.; Bekermann, D.; Gasparotto, A.; Gavagnin, M.; Maccato, C.; Tondello, E.; Bontempi, E.; Depero, L. E.; Sada, C. *CrystEngComm* **2011**, *13*, 3670−3673.
(34) Bekermann, D.; Ludwig, A.; Toader, T.; Maccato, C.; Barreca, D.; Gasparotto, A.; Bock, C.; Wieck, A. D.; Kunze, U.; Tondello, E.; Fischer, R. A.; Devi, A. *Chem. Vap. Deposition* **2011**, *17*, 155−161.
(35) Kim, H. R.; Choi, K. I.; Kim, K. M.; Kim, I. D.; Cao, G. Z.; Lee, J. H. *Chem. Commun.* **2010**, *46*, 5061−5063.
(36) Trinh, T. T.; Tu, N. H.; Le, H. H.; Ryu, K. Y.; Le, K. B.; Pillai, K.; Yi, J. *Sens. Actuators, B* **2011**, *152*, 73−81.
(37) Kakati, N.; Jee, S. H.; Kim, S. H.; Oh, J. Y.; Yoon, Y. S. *Thin Solid Films* **2010**, *519*, 494−498.
(38) Chougule, M. A.; Sen, S.; Patil, V. B. *Ceram. Int.* **2011**, in press; doi: 10.1016/j.ceramint.2011.11.036.
(39) Al-Hardan, N. H.; Abdullah, M. J.; Abdul Aziz, A.; Ahmad, H.; Low, L. Y. *Vacuum* **2010**, *85*, 101−106.